Exploring the cellular and tissue uptake of nanomaterials in a range of biological samples using multimodal nonlinear optical microscopy

Exploring the cellular and tissue uptake of nanomaterials in a range of biological samples using multimodal nonlinear optical microscopy

Helinor J Johnston [1*], Rabah Mouras [2,3 *], David M Brown [1], Alistair Elfick [2], Vicki Stone [1]

[1] Nano Safety Research Group, School of Life Sciences, Heriot-Watt University, Edinburgh, EH14 4AS, UK

[2] Institute for BioEngineering, University of Edinburgh, The King's Buildings, Edinburgh EH9 3JL, UK

[3] Department of Physics & Energy, Materials and Surface Science Institute, University of Limerick, Limerick, Ireland

*corresponding authors; h.johnston@hw.ac.uk , tel: +44 (0)131 451 3303. Fax: +44 (0)131 451 3009, Rabah.Mouras@ul.ie, +353 (0) 61 234 162

Abstract

The uptake of nanomaterials (NMs) by cells is critical in determining their potential biological impact, whether beneficial or detrimental. Thus, investigation of NM internalisation by cells is a common consideration in hazard and efficacy studies. There are currently a number of approaches that are routinely used to investigate NM-cell interactions, each of which have their own advantages and limitations. Ideally, imaging modalities used to investigate NM uptake by cells should not require the NM to be labelled (e.g. with fluorophores) to facilitate its detection. We present a multimodal imaging approach employing a combination of label-free microscopies that can be used to investigate NM-cell interactions. Coherent anti-Stokes Raman scattering (CARS) microscopy was used in combination with either two-photon photoluminescence (TPPL) or four-wave mixing (FWM) to visualise the uptake of gold or titanium dioxide NMs respectively. Live and fixed cell imaging revealed that NMs were internalised by J774 macrophage and C3A hepatocyte cell lines (15-31μg/ml). Sprague Dawley rats were exposed to NMs (intratracheal instillation, 62μg) and NMs were detected in blood and lung leukocytes, lung and liver tissue, demonstrating that NMs could translocate from the exposure site. Obtained data illustrate that multimodal nonlinear optical microscopy may help overcome current challenges in the assessment of NM cellular uptake and biodistribution. It is therefore a powerful tool that can be used to investigate unlabelled NM cellular and tissue uptake in three dimensions, requires minimal sample preparation, and is applicable to live and fixed cells.

Keywords: nanomaterial, uptake, microscopy, CARS, imaging, biodistribution

Introduction

Investigating the uptake of diverse forms of nanomaterials (NMs) (e.g. metal oxides, metals, polymers, and carbon based structures) by cells and tissues is critical in determining their potential biological impact, whether beneficial or detrimental. The uptake of NMs by cells may be a requirement for their toxicity, and so visualising NM-cell interactions is often a key component of in hazard studies. Furthermore, an understanding of NM biodistribution in the body is essential to inform the design of hazard studies (e.g. to identify potential target sites of NM toxicity) and to evaluate the longevity of NMs in the body following exposure. The increased development of nanomedicines and nano-scale medical devices also requires that a better understanding of their cellular uptake and biodistribution is obtained prior to their widespread use in order to ensure they are targeted to the required site in the body, interact with specific target cells, and that they do not stimulate adverse health effects. Imaging the uptake of NMs by cells and tissues is therefore now a routine consideration in hazard and efficacy investigations for NMs. Ideally, imaging modalities used to examine NM-cell interactions should not require the NM to be modified (e.g. with fluorophores) to facilitate NM detection, should involve minimal sample processing, be applicable to fixed or live cells, be able to confirm that NMs are internalised into the cell interior, and should be able to quantify NM uptake.

Probing interactions between NMs and cells has routinely been investigated using fluorescent NMs. The uptake of NMs such as fluorescent polystyrene beads and quantum dots by a variety of cell and tissue types including; macrophages [1,2], hepatocytes [3], red blood cells [4], fibroblasts [5], keratinocytes [6], lung tissue [2] and skin tissue [7] has been investigated previously. Confocal microscopy has been frequently used as it is applicable to fixed and live cells, and allows images to be taken in different focal planes to confirm NM internalisation into the cell interior. However, few forms of intrinsically fluorescent NMs exist, and thus NMs have been labelled with fluorescent tags in order to enable their visualisation (e.g. [8]). The addition of fluorescent labels may alter NM physico-chemical characteristics and thus behaviour, many fluorescent tags are not stable, they may be chemically or photo-bleached, and become detached (e.g. 9-11). Accordingly, it is desirable to use imaging modalities that do not require NM modification to enable their detection.

For non-fluorescent NMs there are a number of approaches which have been used to detect NM-cell interactions, each of which have their own advantages and limitations. The unique optical properties exhibited by NMs can be exploited when imaging their uptake by cells. For

example, ultrafine carbon black and carbon nanotubes can be visualised due to their black colour using bright-field light microscopy (e.g. [12-14]). However, the resolution of light microscopy is not sufficient to identify single NMs, it is difficult to distinguish between NMs that are internalised by cells and those that are attached to the cell surface and does not permit the assessment of NM sub-cellular location.

As some NMs can scatter light, dark-field microscopy can be used to image their internalisation by cells. This technique has been used to visualise a variety of NM types including gold [15, 16], and TiO_2 [17]. This technique has the advantage that the NMs do not need to be modified to enable their detection, however, the usefulness of dark field microscopy relies on the inherent light scattering properties of NMs [17], and so is not applicable to all NMs, and may vary with the physico-chemical form of the NM [18]. A combination of dark field microscopy and confocal microscopy can enable the internalisation of NMs by cells to be confirmed as confocal microscopy can image in 3 dimensions [17]. Alternatively, images taken at different focal planes of a cell have been used to establish whether NMs are taken into the cell interior or remain at the cell surface [15].

Transmission electron microscopy (TEM) has sufficient resolution to image individual NMs, and has been used to successfully image the uptake and sub-cellular localisation of NMs, and evaluate the mechanism of NM uptake in a variety of cell types and tissues including; macrophages [4], hepatocytes [19], fibroblasts [20], skin [21], and intestine [22]. However, there are often difficulties in discriminating NMs from cellular structures. This has been overcome through the use of TEM with other imaging modalities (e.g. dark field microscopy) to enhance contrast and therefore aid the visualisation of NMs [23]. In addition, TEM can be coupled to other techniques to confirm NM uptake by performing an elemental analysis to produce a more informative image [24-30]. Yet of general concern is that TEM sample preparation may introduce artefacts, is very time intensive, costly, and cannot be used to perform imaging studies with live cells [17].

CARS microscopy is a multi-photon imaging technique which allows cells to be imaged without requiring the use of extrinsic labels such as fluorophores [31]. CARS microscopy is suitable for imaging unstained biological samples in real time with high three-dimensional (3D) spatial resolution and requires minimal sample processing. CARS microscopy utilises a resonant form of Raman scattering, where chemical bonds in molecules are stimulated into a vibrational state characteristic of their chemical structure. It is a third order nonlinear optical process in which

molecular vibrations are driven coherently through stimulated excitation by pulsed lasers. Due to the nonlinear nature of the process the signal is greatly amplified over traditional Raman spectroscopy, thus allowing imaging at high speed and high sensitivity. In the CARS process two laser pulses are required; a pump beam at frequency ω_p and a Stokes beam at frequency ω_s which interact with the sample in a four-wave mixing (FWM) process. When the frequency $\omega_p - \omega_s$ matches that of a Raman active molecular vibration, the chemical bonds are excited resonantly generating a strong anti-Stokes signal at $\omega_{as}=2\omega_p-\omega s$. This enables contrast to be derived from intrinsic sample properties (e.g. a stretching vibration in methyl moieties is highly characteristic of lipids), removing the need to label the sample to visualise the cell structure.

CARS microscopy is not, however, background-free; the non-resonant background, an inherent electronic contribution to the CARS signal that is independent of the Raman shift, can overwhelm the vibrational contrast. For most applications in CARS microscopy investigators strive to minimise the non-resonant contributions and hence optimise image contrast. In this study, we will exploit this non-resonant signal to generate contrast from metal and metal oxide NMs. Metallic NMs are known to have large non-linear susceptibilities that are enhanced by two-photon electronic resonance, making them efficient candidates for four-wave mixing process, like CARS microscopy. TiO_2 NMs show a large FWM signal, whilst Au NMs exhibit two-photon photoluminescence (TPPL) which is enhanced by surface plasmons. These two nonlinear optical phenomena were exploited to localise different types of NMs within biological samples at the cellular level.

Despite its ability to image a diverse array of unmodified NMs, CARS microscopy has only been used to a very limited extent to image NM interaction with cells. However, existing studies have demonstrated the usefulness of CARS microscopy in imaging; the uptake of metal oxide NMs (e.g. TiO_2, ZnO, and CeO_2) by fish (gills) [32, 33], the uptake of SWCNTs by the sediment dwelling organism *Arenicola marina* (lugworm) [34], and the internalisation of gold NMs by macrophages [35] and epidermal keratinocytes and squamous carcinoma cells [36]. The majority of published studies which have investigated NM-cell/tissue interactions using CARS microscopy have focused on environmental organisms. The usefulness of this imaging modality to investigate NM uptake by more diverse (mammalian) cells and tissues for the hazard and efficacy assessment of NMs has not been rigorously assessed.

This study assessed the suitability of using CARS microscopy, in combination with other imaging modalities (termed NLO microscopy), to investigate NM-cell interactions.. Importantly,

NMs were not modified to enable their detection, and samples (cells and tissues) investigated were not stained to visualise cell or tissue structure (i.e. imaging is label free). The study aimed to assess whether NLO microscopy could be used to i) investigate the uptake of unlabelled NMs, of varied physico-chemical properties, by cells in 3 dimensions (i.e. in order to confirm NM uptake into the cell interior), and ii) assess the uptake of unlabelled NMs by live and fixed cells, and fixed tissues in order to demonstrate that NLO microscopy is a useful tool that can be applied to a range of biological samples obtained from *in vitro* and *in vivo* studies. The mechanism of NM uptake and their intracellular fate was not investigated, and NM cellular uptake was not quantified. In the first instance the uptake of NMs (TiO_2 and gold (Au)) by macrophage and hepatocyte cell lines was evaluated in fixed and live cells. NM uptake by tissues (lung and liver) and leukocytes (obtained from lung or blood) was then investigated following the exposure of rats to NMs via intratracheal instillation. The study focused on cell types that are known to be capable of internalising NMs, and organs known to accumulate NMs. More specifically, there is a wealth of evidence available which illustrates that macrophages located in different tissues (e.g. lung, liver) accumulate NMs following the exposure of rodents (e.g. [4, 37-40]) and that macrophage cell lines and primary cells are capable of internalising NMs *in vitro* (e.g. [1]). The liver is a recognised site of NM accumulation *in vivo* (e.g. [41]), and there is evidence that hepatocytes are able to internalise NMs *in vitro* [3, 19, 42]. NM concentrations of up to 31µg/ml were selected for *in vitro* studies, and a dose of 62µg/animal was chosen for *in vivo* experiments. The choice of NM concentration/dose was based on our previous experience of testing the toxicity of these exact NM types to hepatocyte and macrophage cell lines and rodents (e.g. [19, 42-45]). Similarly, the time points (2-4 hours) used to assess the uptake of NMs by cells *in vitro* were based on our previous experience of investigating the uptake of NMs by macrophages and hepatocytes (e.g. [1,3]). For *in vivo* studies, an acute, 24 hour exposure was selected, and based on existing evidence of NM toxicity and biodistribution following pulmonary exposure (e.g. [41]).

Experimental Details

All materials were purchased from Sigma-Aldrich (Poole, UK) unless otherwise stated.

NM Panel

TiO_2 NMs (NRCWE001, size: 10nm) were a kind gift from Prof. Hakan Wallan (NRCWE, Denmark). Gold unfunctionalised NMs (20nm) were purchased from Melorium Technologies (Rochester, USA). The physico-chemical properties of the NMs used in this study have been

previously characterised [16, 37-39]. Briefly, the size of TiO_2 NMs, as measured by TEM was 80-400nm and NMs had a hydrodynamic diameter of 200nm when dispersed in cell culture medium [19, 44, 45]. Au NMs had a hydrodynamic diameter of 140nm when dispersed in complete cell culture medium and primary particle size of 85-110nm as measured by SEM [43].

NM preparation

TiO_2 NMs were supplied as dry powders. Au NMs (20nm) were supplied in an aqueous suspension. The NMs were dispersed in distilled water with 2% FCS at a concentration of 1mg/ml, and then sonicated (in a bath sonicator) for 16 minutes following a protocol developed during the FP7 funded project ENPRA [46]. NMs were then diluted immediately in biological medium (varied according to whether *in vitro* or *in vivo* experiments were being conducted) to the required concentration.

J774 cell culture and treatment

The murine macrophage cell line J774.1 (European collection of cell cultures (ECACC)) was cultured in RPMI 1640 medium supplemented with 10% heat-inactivated FCS, 2 mM L-glutamine, 100 U/ml penicillin/ streptomycin; termed complete macrophage cell culture medium (all obtained from Life Technologies, Paisley, UK) at 37°C in 5% CO_2. For fixed cell imaging, cells were scraped from the culture flasks and seeded at a concentration of 5 x 10^4 cells/ml into Petri dishes (volume of 1ml) and incubated for 24 h at 37°C in 5% CO_2. The medium was then removed, and the cells were treated with NMs (suspended in complete macrophage cell culture medium) at a concentration of 31µg/ml for 4 hours. Cells were then washed with medium and fixed with 10% formaldehyde at 4^{o}C for one hour. The cells were then washed with phosphate buffered saline (PBS) and stored at 4^{o}C (in PBS).

For live cell imaging J774 cells were seeded at a concentration of 5 x 10^4 cells/ml into Petri dishes (at a volume of 1ml) and incubated at 37°C, in 5% CO_2. After 24 hours cells were washed with complete macrophage cell culture medium. The cells were then exposed to NMs at a concentration of 15µg/ml (in complete macrophage cell culture medium) and imaged immediately over a period of 2 hours.

C3A cell culture and treatment

The human hepatoblastoma C3A cell line was maintained in Minimum Essential Medium Eagle (MEM) with 10% FCS, 2 mM L-glutamine, 100 U/ml penicillin/ streptomycin, 1 mM sodium pyruvate and 1% nonessential amino acids (termed complete hepatocyte cell medium) at 37°C and 5% CO_2 (all reagents obtained from Life Technologies, Paisley, UK). For fixed cell imaging, cells were removed from cell culture flasks using trypsin and seeded at a concentration of 5 x 10^4 cells/ml into Petri dishes (volume of 1ml) and incubated for 24 h at 37°C. The medium was then removed, and the cells were treated with NMs (suspended in hepatocyte cell medium) at a concentration of 15 or 31µg/ml for 4 h. Cells were then washed with cell culture medium and fixed with 10% formaldehyde at 4^{o}C for one hour. The cells were then washed with PBS, fixed with 10% formaldehyde at 4^{o}C for one hour and stored at 4^{o}C (in PBS).

For live cell imaging, C3A cells were seeded at a concentration of 5 x 10^4 cells/ml into Petri dishes (volume of 1ml) and incubated at 37°C, in 5% CO_2. After 24 hours incubation at 37°C, cells were washed with complete hepatocyte cell culture medium. The cells were then exposed to NMs at a concentration of 15 (TiO_2) or 31 (Au) µg/ml (in complete hepatocyte cell culture medium) and imaged immediately over a period of 2 hours.

***In vivo* studies**

Male Sprague Dawley rats (3 months old) were obtained from Biomedical Research Resources, Royal Infirmary Edinburgh (Edinburgh, UK). The research was conducted in accordance with UK Home Office regulations. Food and water were available *ad libitum*. Rats were anaesthetised with isoflurane and instilled intratracheally with a single dose of NM suspended in 0.5ml saline to give a dose of 62µg/animal. All animals recovered fully after this treatment and showed no ill effects. After 24 hours, rats were sacrificed. Blood was removed from the abdominal aorta and collected into heparin blood tubes. The lungs were cannulated and lavaged with 4x8ml volumes of saline and the lavageate pooled into a single tube (termed bronchoalveolar lavage (BAL)). Lung and liver tissues were harvested and fixed in 10% formaldehyde after which the tissues were processed for paraffin wax histology and sectioned (5µm tissue sections). Tissues were de-waxed prior to imaging.

To prepare BAL leukocytes for imaging, the BAL fluid was centrifuged at 850g for 2 minutes. The supernatant was removed and the cells resuspended in macrophage complete cell culture medium. Cells were seeded at a concentration of 0.5 x 10^6 cells/ml in Petri dishes (1ml) and

incubated at 37^{o}C for 1 hour to allow the cells to adhere. Cells were then washed with cell culture medium to remove non-adherent cells and fixed with 10% formaldehyde at 4^{o}C for one hour. The cells were then washed with PBS and stored at 4^{o}C (in PBS) until required for imaging.

To prepare blood leukocytes for microscopy red blood cells were lysed with lysis buffer (0.15M ammonium chloride, 0.01M sodium bicarbonate, 1mM EDTA (disodium salt)). The suspension was centrifuged at 250g for 10 minutes at 4^{o}C. The cell pellet was washed with PBS and the cells then centrifuged at 250g for 10 minutes at 4^{o}C. The cell pellet was then resuspended in 2ml complete macrophage cell culture medium. Cells were seeded at a concentration of 0.5 x 10^{6} cells/ml in Petri dishes (1ml) and incubated at 37^{o}C for 1 hour to allow the cells to adhere. The cells were fixed with 10% formaldehyde at 4^{o}C for one hour and then washed with PBS and stored (in PBS) at 4^{o}C.

Multimodal microscope

The microscope setup used in this study has been described previously [47]. Briefly, a mode-locked Nd:YVO_4 laser source (PicoTrain, High-Q laser) produces the Stokes pulse (6 ps, 1064.4 nm) and a 5 ps, frequency-doubled, 532 nm beam, which was used to pump a picosecond optical parametric oscillator (OPO) (Levante Emerald, APE). The OPO delivers a signal tunable in the range ~700 - 1000 nm that was used as a pump in the CARS process. The two beams are combined in a collinear geometry and focused on the sample using a high transmission x25 water immersion objective (XL Plan N, Olympus) with 1.05 numerical aperture (NA). A laser-scanning, confocal, inverted optical microscope (C1 Eclipse, Nikon BV, Amsterdam, Netherlands) is used to acquire images. Sets of appropriate short-pass and band-pass filters were used to transmit the desired nonlinear signals. The laser power at the sample was 12 mW and 8 mW for the pump and Stokes beams, respectively. A schematic diagram of the multimodal microscope used is presented in Figure 1.

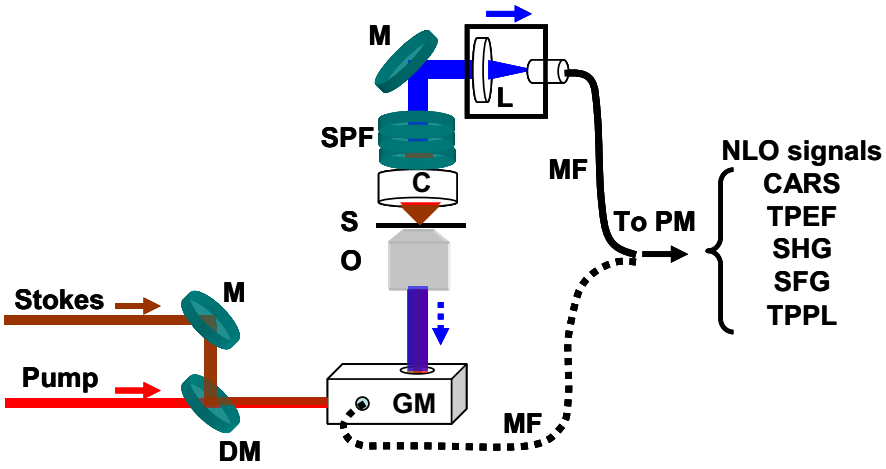

Figure 1: *Experimental set-up of the multimodal microscope. In this study CARS microscopy was used in combination with FWM to image TiO_2 NMs, and with TPPL to image Au NMs (termed nonlinear optical (NLO) microscopy). Two-photon excitation fluorescence (TPEF), second harmonic generation (SHG), and sum frequency generation (SFG) and alternate modes of NLO accessible to the microscope but not considered in this study.*

Cell structure was visualised via the imaging of lipids using CARS microscopy (the CH_2 vibration at 2845 cm^{-1} of lipids was excited); the pump laser was tuned to 817 nm (12240 cm^{-1}) with the Stokes beam 1064.4 nm (9395 cm^{-1}), giving a CARS signal at 662.9 nm (15085 cm^{-1}). Short-pass filters (SPF) (800SP, 750SP and 700SP), and a band-pass filter (660/13, FWHM = 13 nm) were used to collect the CARS signal. CARS microscopy was combined with additional NLO imaging modes to investigate the presence of NMs in cells. The approach used depended on the NM under investigation; CARS microscopy was combined with FWM to image TiO_2 NMs or with TPPL to image Au NMs. z stacks were performed to confirm the internalisation of NMs by cells. All acquired images were 512x512 pixels in size and the acquisition time was 1s per image.

Results and Discussion

NM uptake by macrophage and hepatocyte cell lines

In the first instance fixed J774 macrophage and C3A hepatocyte control cells (not exposed to NMs) were imaged using NLO microscopy. In order to visualise cell structure the pump and Stokes beams of the CARS microscope were tuned so that the frequency difference matched the Raman vibration of CH_2 in lipids at 2845 cm^{-1}. CARS microscopy was performed in combination with FWM and TPPL microscopy when imaging control cells to confirm that cellular

structures did not give a FWM or TPPL signal in the absence of NMs (Figure 2). Using this approach we were able to visualise the cell structure of unlabelled macrophages and hepatocytes, with bright spots in the images corresponding to lipid droplets (Figure 2). No FWM or TPPL signal was observed in the absence of NMs.

Multimodal microscopy images of J774 macrophages and C3A hepatocytes that had been exposed to TiO_2 or Au NMs for 4 hours then fixed and imaged, are presented in Figure 2. The images demonstrate that macrophages and hepatocytes were able to accumulate TiO_2 and Au NMs following a 4 hour exposure (Figure 2). NMs accumulate in the cytosol, with no localisation in the nucleus observed. Confirmation of internalisation of both NM types by cells into the cell interior is confirmed in the side panels of the images (yz and xz planes) (Figure 2).

TiO_2 NMs were detectable inside a large proportion of the macrophages imaged, but a smaller proportion of hepatocytes were observed to internalise TiO_2 NMs. In fact, the concentration of TiO_2 NMs in the hepatocyte exposures was reduced to 15μg/ml due to the large number of background NMs evident when a concentration of 31μg/ml was tested, which obscured visualisation of the cells (data not shown). This is likely to derive from the fact that macrophages are professional phagocytes, whereas hepatocytes are not. Therefore the mechanism of entry of NMs into cells and the extent of NM uptake is likely to vary according to the cell type under investigation (i.e. whether it is phagocytic or non-phagocytic). For an overview of the mechanisms by which NMs enter cells please refer to the following reviews [48-50]. Macrophages and hepatocytes were also capable of accumulating Au NMs following a 4 hour exposure (Figure 2). Uptake of Au NMs was observed in both cell types, however the uptake of Au NMs occurred to a lesser extent than that observed for TiO_2 NMs. The quality of images obtained in this study is comparable to those acquired using confocal microscopy when visualising the uptake of fluorescent polystyrene NMs by stained macrophages [1] and hepatocytes [3] in previous studies. Importantly, unlike confocal microscopy, NLO microscopy has the advantage that it does not require the use of fluorescent NMs and cells do not have to be labelled to visualise their cell structure, and so sample preparation time is reduced.

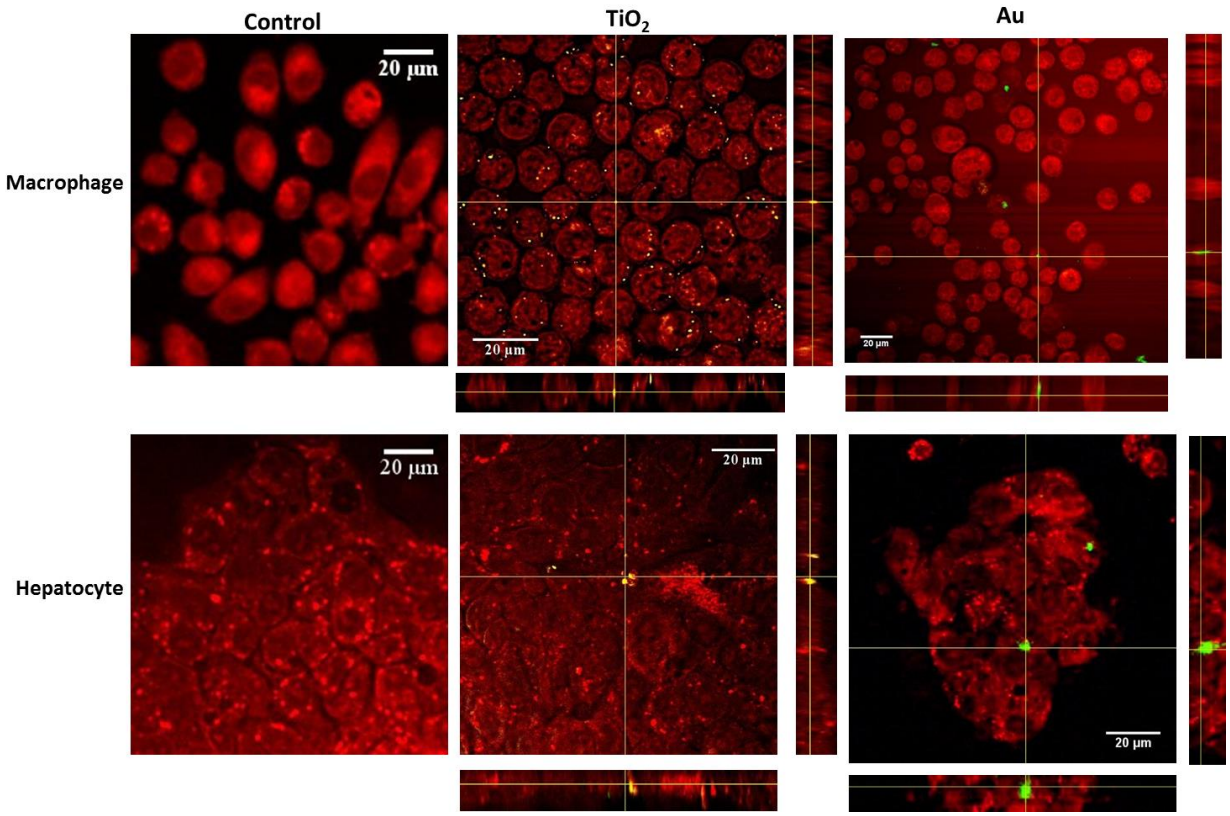

Figure 2. *NM uptake by macrophages and hepatocytes in vitro. J774 macrophages (top panel) and C3A hepatocytes (bottom panel) were exposed to complete cell culture medium (control), TiO_2 or Au NMs (green) for 4 hours, fixed and then imaged. Images were obtained using CARS microscopy at the Raman frequency 2845 cm^{-1} corresponding to the CH_2 vibration in lipids to visualise cell structure (red) in combination with FWM (a frequency at 3060 cm^{-1}) and TPPL (frequency of 609 nm) microscopy. Side panels present z-sections along the x and y planes and show the 3D distribution of cells confirming that NMs were present in the cell interior.*

Intensity profiles (along the blue lines) are presented alongside images of NM uptake by cells (fixed J774 macrophages and C3A hepatocytes) in Figure 3. Peaks in the intensity profiles represent NMs (or NM agglomerates/aggregates) in cells. Intensity profiles (along the blue lines) clearly demonstrate the contrast between cells (lipid) and NMs.

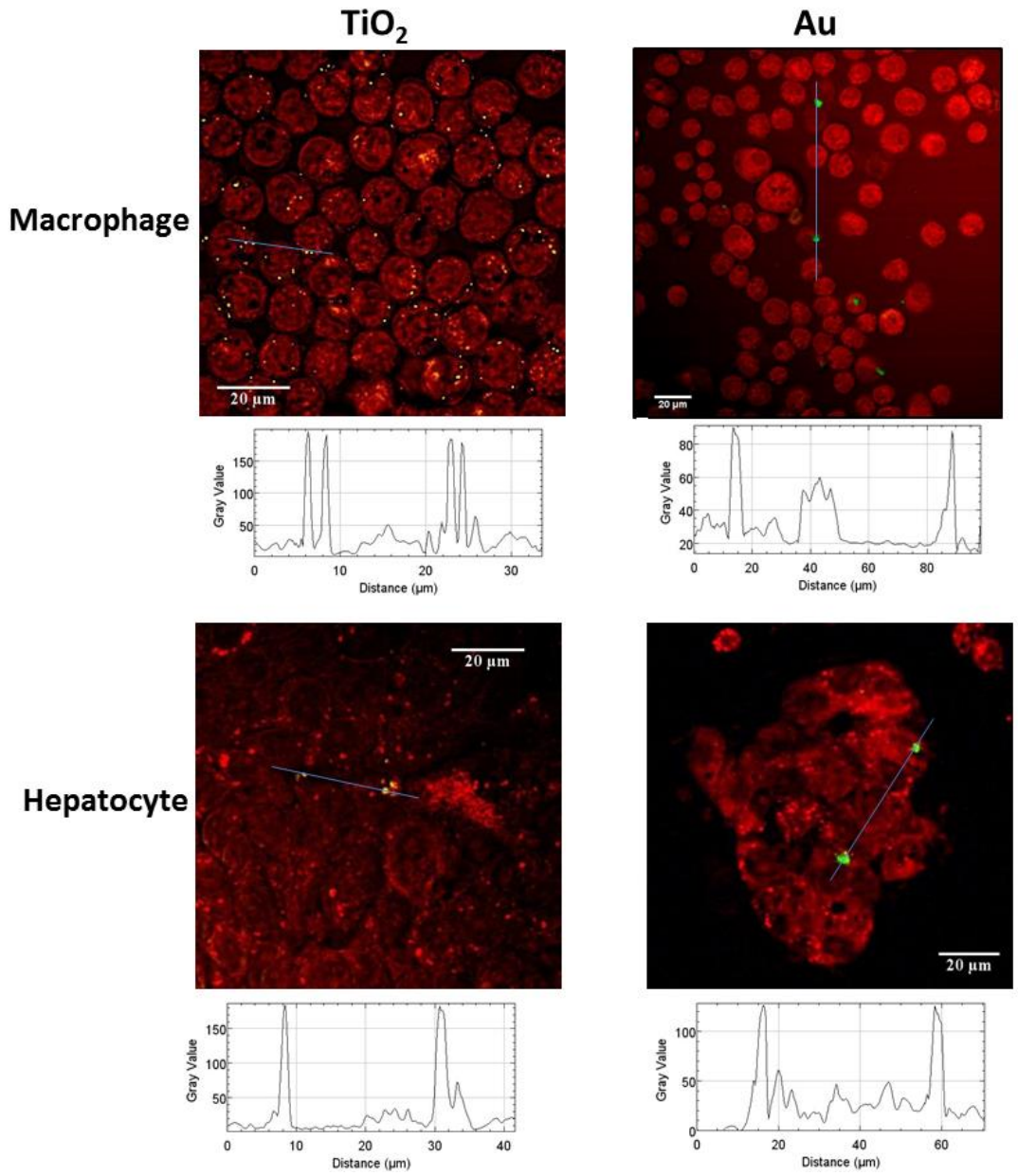

Figure 3. Intensity profiles (along the blue line) of NM uptake (green) by macrophages and hepatocytes (red) (in fixed samples). Contrast between J774 macrophage and C3A hepatocyte cells (lipid) and TiO_2 or Au NMs is demonstrated in the intensity profiles. Images were obtained using NLO microscopy (please refer to figure 2) and intensity profiles generated using Image J.

Imaging of live cells confirmed that J774 macrophages and C3A hepatocytes were able to internalise TiO_2 and Au NMs (Figure 4). The images presented are taken at the end of the exposure time of 2 hours (Figure 4). It was demonstrated that TiO_2 NMs were internalised by both macrophages and hepatocytes (Figure 4). NMs are localised in the cytosol, with no

accumulation in the nucleus observed. Confirmation of NM uptake by cells can be visualised on the side panels of the images (yz, and xz planes). Au NMs were also internalised by macrophages and hepatocytes, but to a lesser extent than TiO_2 NMs.

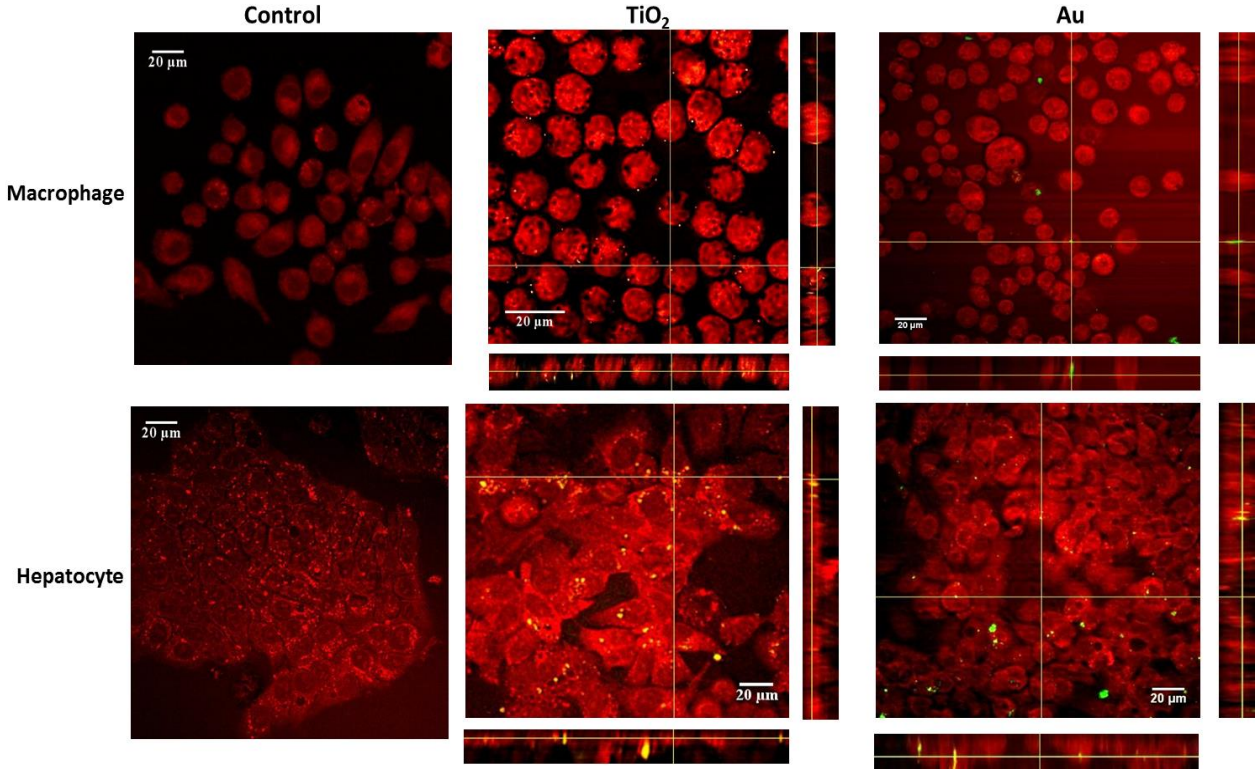

Figure 4. *J774 macrophage (top panel) and C3A hepatocyte (bottom panel) cell lines were exposed to cell culture medium (control), TiO_2 or Au NMs for 2 hours.* The images presented were taken from live cells at the end of the 2 hour exposure time. *Visualisation of the cell structure (red) was obtained using CARS microscopy at the Raman frequency 2845 cm^{-1} which corresponds to the CH_2 vibration in lipids. To image TiO_2 NMs (green), FWM mixing at a frequency at 3060 cm^{-1} was performed. Au NMs (green) were imaged by TPPL microscopy at 609 nm. Side panels present z-sections along the planes show the 3D distribution of cells confirming that the NMs were present in the cell interior.*

Obtained data indicate that TiO_2 NMs were more avidly taken up by both macrophage and hepatocyte cell lines than Au NMs. Therefore, despite being administered at the same mass dose, there were less Au NMs taken up by cells when compared to TiO_2 NMs. Gold is a dense metal in comparison to TiO_2 and consequently fewer Au NMs are present in a similar mass of NM. This may explain why there were less Au NMs present in the cells. Alternatively, TiO_2 NMs

may be more readily phagocytosed than Au NMs. The aim of this study was not to investigate the relationship between NM physico-chemical properties and uptake. Instead a focus was placed on determining whether multimodal NLO microscopy was applicable to NMs that varied with respect to their composition. However, it is known that the optical properties of NMs are affected by their physico-chemical properties such as size, and shape (e.g [18]). Thus, as there is a huge diversity of NMs under development and use future studies could obtain a panel of NMs of the same composition but of varied size, shape or surface charge and determine if NM physico-chemical properties affects how easily they can be detected using multimodal NLO microscopy, and to determine the impact of physico-chemical properties on NM uptake by cells. Of interest is that existing studies have demonstrated that NM size, shape, agglomeration status and surface properties impact on their uptake by cells (e.g. [1, 3, 9, 26, 51]). In addition, knowledge of the properties of NMs which control uptake can be exploited in the design of nanomedicines in the future (reviewed in [49, 52]). Furthermore, future studies could explore whether NLO microscopy is suitable for assessing 'mixed' NM exposures (i.e. when cells / tissues are exposed to more than one NM at a time), as well as its applicability to more complex NMs (e.g. nanoclays, nanocomposites). Whilst the (lived and fixed cell) images presented confirm that Au and TiO_2 NMs were internalised into the cell interior (in both macrophages and hepatocytes), the mechanism of uptake and intracellular fate of NMs was not investigated. However, it is possible to use NLO microscopy to assess the sub-cellular location of NMs. For example fluorescent stains could be used to enable the visualisation of specific organelles (e.g. lysosomes), and the co-location of NMs with these structures visualised using a combination of fluorescence and CARS microscopy. Furthermore, it is possible to identify specific organelles in cells/tissues without the requirement for fluorescent stains, using CARS microscopy alone (reviewed by [53]) or in combination with other imaging modalities [54, 55]. For example, the nucleus and mitochondria of cells have been imaged previously using CARS microscopy [56, 57]. The ability to image a more diverse array of cellular organelles using multimodal NLO microscopy could therefore be the focus of future studies, as well as investigation of the intracellular fate of NMs. However, this approach may be limited by the target organelle under investigation, as CARS microscopy has been most widely applied to visualise lipids due to the stronger signal associated with C-H bond stretches in lipids and thus its applicability to other structures requires further investigation [54], and investigators will also need to consider whether the spatial resolution of NLO microscopy is adequate to image smaller organelles (<300nm in size).

The detection of NM uptake by cells using microscopy has been performed in nanotoxicology and nanomedicine studies to gain a better understanding of the sub-cellular location and mechanism of NM uptake into cells, and to identify what the potential consequences of NM uptake may be (beneficial and detrimental). This study did not quantify the uptake of NMs by cells as it was not possible to image single particles, as the resolution of the NLO microscope is ~250-300 nm. However to better understand NM-cell interactions it would be of interest to quantify NM uptake by cells (i.e. number, mass or surface area of NMs internalised by a cell) [58, 59]. Currently there is a lack of knowledge regarding how the exposure dose of NMs is related to the cellular NM dose for *in vitro* experiments [59, 60]. However information on the cellular content (internal dose) of NMs is required to better design and interpret the findings of *in vitro* NM toxicity experiments [61], and to detect the targeted delivery of NMs into cells in therapeutic and diagnostic settings [62]. Although there is a desire to quantify NM uptake by cells, this has been a challenging area of activity. To date, flow cytometry has been used to quantify the uptake of fluorescent NMs by cells (e.g. [1, 63, 64]), and to a more limited extent to investigate the uptake of non-fluorescent NMs (e.g. [65, 66]). In addition, confocal microscopy has been used to quantify the uptake of fluorescent NMs, based on fluorescent intensity measurements (e.g. [67]). However these approaches are typically limited to fluorescent NMs. Alternatively, the number of NMs internalised by cells has been assessed using electron microscopy, which requires the number of NMs internalised to be counted by the investigator (e.g. [63, 68]). The resolution of NLO microscopy is sufficient to image particles that are ~250-300 nm in size. Thus the ability of NLO microscopy to quantify the number of NMs internalised by cells could be explored in future studies, although it is likely that it will be limited to larger particles or NMs that are agglomerated or aggregated.

NM uptake by cell and tissue samples obtained from in vivo studies

Rats were exposed to NMs via intratracheal instillation and leukocytes isolated from blood and BAL 24 hours post exposure. It was challenging to detect NM uptake by blood and BAL leukocytes, and particularly difficult for blood leukocytes. The uptake of TiO_2 NMs was observed in alveolar BAL and blood leukocytes (Figure 5). No Au NMs were detected in BAL or blood derived leukocytes (data not shown). A more comprehensive study is needed in order to investigate the interaction of NMs with leukocytes derived from blood and BAL. More specifically, future studies could use a range of time points to investigate if NM uptake by these

cell types changes over time as only one time point was investigated in this study. In addition rats could be exposed to a higher dose of NMs to increase the likelihood of detection.

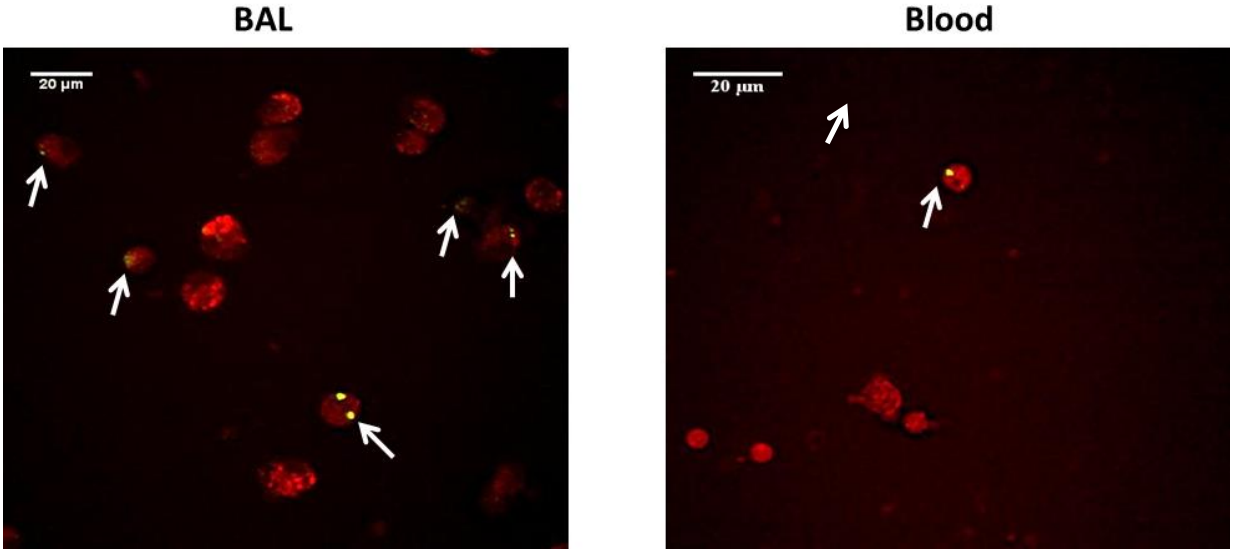

Figure 5. *Rats were exposed to TiO_2 NMs (62µg) via intratracheal instillation. 24 hours post exposure rats were sacrificed, a BAL performed, and blood was taken. Leukocytes were then isolated from BAL fluid and blood, fixed and imaged using NLO microscopy. Visualisation of the cell structure (red) was obtained using CARS microscopy at the Raman frequency 2845 cm^{-1} which corresponds to the CH_2 vibration in lipids. To image TiO_2 NMs (green), FWM mixing at a frequency at 3060 cm^{-1} was performed. White arrows indicate which cells had internalised TiO_2 NMs.*

The structure of unstained lung and liver (fixed) tissue obtained from control rats (not exposed to NMs) were imaged via the visualisation of lipids (Figure 6). The images of control tissues were captured using multimodal NLO microscopy (combination of CARS, FWM and TPPL microscopy) to ensure that cellular structures did not give an FWM or TPPL signal in the absence of NMs (Figure 6). Imaging of lipids enabled tissue structure to be visualised, with no FVM or TPPL signal observed in the absence of NMs. Following intratracheal instillation, TiO_2 and Au NMs were detected in the alveolar region of the rat lung (Figure 6). TiO_2 and Au NMs were also detected in the liver tissue following intratracheal instillation (Figure 6). Obtained data suggests that both NM types investigated were able to translocate from the lungs into the circulation and then accumulated in the liver. Assessment of the biodistribution of unmodified NMs has been a great challenge due to the necessity of detecting small quantities of NMs at a variety of target sites. As a consequence, biodistribution studies conducted to date have

focused on assessment of the accumulation of inherently fluorescent (e.g. quantum dots, silica) or modified (e.g fluorescently tagged or radiolabelled) NMs (e.g. [26, 41, 69-71]). In order to assess whether multimodal NLO microscopy could offer advantages over current approaches used to assess NM biodistribution, future studies should use a wider range of NM doses to identify the sensitivity of this approach, and whether tissue accumulation can be quantified. Evaluation of the biodistribution and accumulation of NMs following exposure via different exposure routes (e.g. ingestion) and in a wider range of tissues could also be considered. Whilst this study investigated the localisation of NMs in the lung and liver, it did not evaluate the toxicity exhibited by NMs in these tissues. Evidence of uptake of NMs by a tissue does not imply that they will exert toxicity. Accordingly, further studies are required to evaluate the pulmonary and hepatic toxicity of the NMs tested in this study. In fact, the toxicity of these exact NMs has been investigated in hepatic and macrophage *in vitro* models [19, 43-45]

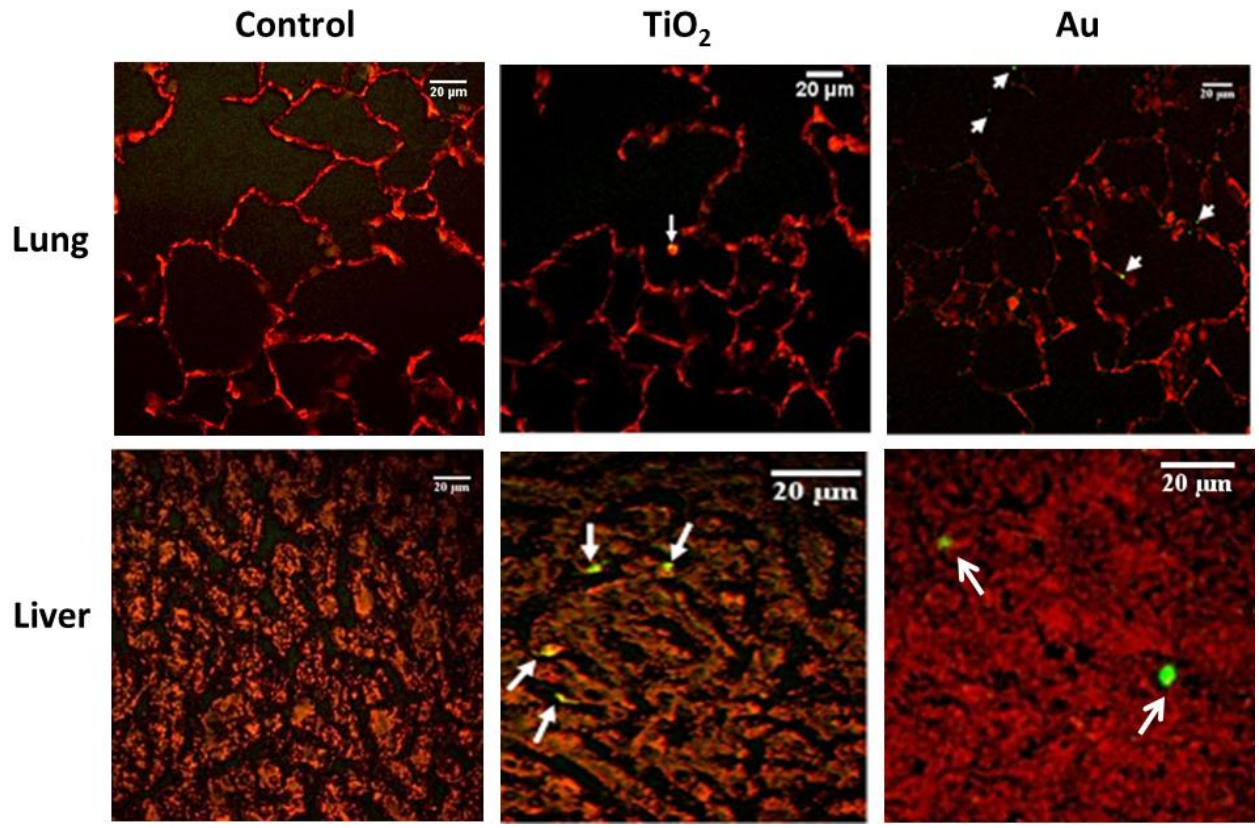

Figure 6. *Uptake of NMs by lung and liver tissue in vivo. Rats were exposed to PBS (control) TiO_2 or Au NMs (62µg) via intratracheal instillation. Rats were sacrificed 24 hours post exposure and lung and liver tissue was removed and fixed. Tissue sections were then imaged using NLO*

microscopy. Visualisation of the tissue structure (red) was obtained using CARS microscopy at the Raman frequency 2845 cm^{-1} which corresponds to the CH_2 vibration in lipids. CARS microscopy was combined with FWM at a frequency at 3060 cm^{-1} to image TiO_2 NMs (green) or TPPL at 609 nm to image Au NMs (green). The localisation of NMs in tissue is indicated by white arrows.

Conclusion

This study has demonstrated that multimodal NLO microscopy is a very promising and powerful technique that can be used to image the uptake of NMs by a variety of unstained cell and tissue types. Multimodal NLO microscopy can be used to investigate NM-cell interactions *in vitro* and *in vivo*, and may also be a useful tool when investigating NM biodistribution. As such we suggest that future studies investigating the efficacy and hazard of NMs *in vitro* and *in vivo* could use this imaging modality to a greater extent. In particular its ability to detect unmodified, non-fluorescent NMs in fixed cells and tissues, and live cells in three dimensions, with minimal sample preparation is greatly appealing.

Conflict of Interest

The authors declare that there are no conflicts of interest.

References

1. Clift MJ, Rothen-Rutishauser B, Brown DM, Duffin R, Donaldson K, Proudfoot L, Guy K, Stone V 2008 *Toxicol Appl Pharmacol* **232** 418

2. Roberts JR, Antonini JM, Porter DW, Chapman RS, Scabilloni JF, Young SH, Schwegler-Berry D, Castranova V, Mercer RR 2013 *Part Fibre Toxicol* **10** 5

3. Johnston HJ, Semmler-Behnke M, Brown DM, Kreyling W, Tran L, Stone V (2010). *Toxicol Appl Pharmacol* **242** 66

4. Geiser M, Rothen-Rutishauser B, Kapp N, Schürch S, Kreyling W, Schulz H, Semmler M, Im Hof V, Heyder J, Gehr P 2005 *Environ Health Perspect* **113,** 1555

5. Mahto SK, Park C, Yoon TH, Rhee SW 2010 *Toxicol In Vitro* **24** 1070

6. Zhang LW, Monteiro-Riviere NA 2009 *Toxicol Sci* **110** 138

7. Ryman-Rasmussen JP, Riviere JE, Monteiro-Riviere NA 2006 *Toxicol Sci* **91** 159

8. Lacerda L, Russier J, Pastorin G, Herrero MA, Venturelli E, Dumortier H, Al-Jamal KT, Prato M, Kostarelos K, Bianco A 2012 *Biomaterials* **33** 3334

9. Swift JL, Cramb DT 2008, *Biophys J* **95** 865

10. Sirimuthu NM, Syme CD, Cooper JM 2011*Chem Commun* **47** 4099

11. Weiss B, Schaefer UF, Zapp J, Lamprecht A, Stallmach A, Lehr CM 2006 *J Nanosci Nanotechnol* **6** 3048

12. Brown DM, Kinloch IA, Bangert U, Windle AH, Walter DM, Walker GS, Scotchford CA, Donaldson K, Stone V 2007 Carbon **45** 1743

13. Poland CA, Duffin R, Kinloch I, Maynard A, Wallace WA, Seaton A, Stone V, Brown S, Macnee W, Donaldson K 2008 *Nat Nanotechnol* **3** 423

14. Sayes CM, Liang F, Hudson JL, Mendez J, Guo W, Beach JM, Moore VC, Doyle CD, West JL, Billups WE, Ausman KD, Colvin VL 2006 *Toxicol Lett* **161** 135

15. Vetten MA, Tlotleng N, Tanner Rascher D, Skepu A, Keter FK, Boodhia K, Koekemoer LA, Andraos C, Tshikhudo R, Gulumian M 2013 *Part Fibre Toxicol* **10** 50

16. Huang X, El-Sayed IH, Qian W, El-Sayed MA 2006 *J Am Chem Soc* **128** 2115

17. Gibbs-Flournoy EA, Bromberg PA, Hofer TP, Samet JM, Zucker RM 2011 *Part Fibre Toxicol* **8** 2

18. Jain PK, Lee KS, El-Sayed IH, El-Sayed MA 2006 *J Phys Chem B* **110** 7238

19. Kermanizadeh A, Pojana G, Gaiser BK, Birkedal R, Bilanicová D, Wallin H, Jensen KA, Sellergren B, Hutchison GR, Marcomini A, Stone V 2013 *Nanotoxicology* **7** 301

20. Coradeghini R, Gioria S, García CP, Nativo P, Franchini F, Gilliland D, Ponti J, Rossi F 2013 *Toxicol Lett* **217** 205

21. Prow TW, Monteiro-Riviere NA, Inman AO, Grice JE, Chen X, Zhao X, Sanchez WH, Gierden A, Kendall MA, Zvyagin AV, Erdmann D, Riviere JE, Roberts MS 2012 *Nanotoxicology* **6** 173

22. Fisichella M, Berenguer F, Steinmetz G, Auffan M, Rose J, Prat O 2012 *Part Fibre Toxicol* **9** 18

23. Rosman C, Pierrat S, Henkel A, Tarantola M, Schneider D, Sunnick E, Janshoff A, Sönnichsen C 2012 *Small* **8** 3683

24. Mortensen LJ, Oberdörster G, Pentland AP, Delouise LA 2008 *Nano Lett* **8** 2779.

25. Mu Q, Hondow NS, Krzemiński L, Brown AP, Jeuken LJ, Routledge MN 2012 *Part Fibre Toxicol* **23** 9

26. Clift MJ, Brandenberger C, Rothen-Rutishauser B, Brown DM, Stone V 2011 *Toxicology* **286** 58

27. Brandenberger C, Clift MJ, Vanhecke D, Mühlfeld C, Stone V, Gehr P, Rothen-Rutishauser B 2010 *Part Fibre Toxicol* **3** 7

28. Gass MH, Porter AE, Bendall JS, Muller K, Skepper JN, Midgley PA, Welland M. 2010 **110** 946

29. Cheng C, Müller KH, Koziol KK, Skepper JN, Midgley PA, Welland ME, Porter AE 2009 *Biomaterials* **30** 4152

30. Al-Jamal KT, Nerl H, Müller KH, Ali-Boucetta H, Li S, Haynes PD, Jinschek JR, Prato M, Bianco A, Kostarelos K, Porter AE 2011 *Nanoscale* **3** 2627

31. Pope I, Langbein W, Borri P, Watson P 2012 *Methods Enzymol* **504** 273

32. Moger J, Johnston BD, Tyler CR 2008 *Opt Express* **16** 3408

33. Johnston BD, Scown TM, Moger J, Cumberland SA, Baalousha M, Linge K, van Aerle R, Jarvis K, Lead JR, Tyler CR 2010 *Environ Sci Technol* **44** 1144

34. Galloway T, Lewis C, Dolciotti I, Johnston BD, Moger J, Regoli F 2010 *Environ Pollution* **158** 1748

35. Garrett N, Whiteman M, Moger J 2011 *Opt Express* **19** 17563

36. Rago G, Bauer B, Svedberg F, Gunnarsson L, Ericson MB, Bonn M, Enejder A 2011 *J Phys Chem B* **115** 5008

37. Ogawara K, Yoshida M, Higaki K, Kimura T, Shiraishi K, Nishikawa M, Takakura Y, Hashida M 1999 *Journal of Controlled Release* **59** 15

38. Semmler-Behnke M, Takenaka S, Fertsch S, Wenk A, Seitz J, Mayer P, Oberdörster G, Kreyling WG 2007 *Environ Health Perspect* **115** 728

39. Sadauskas E, Wallin H, Stoltenberg M, Vogel U, Doering P, Larsen A, Danscher G 2007 *Part Fibre Toxicol* **4** 10

40. Takenaka S, Möller W, Semmler-Behnke M, Karg E, Wenk A, Schmid O, Stoeger T, Jennen L, Aichler M, Walch A, Pokhrel S, Mädler L,Eickelberg O, Kreyling WG 2012 *Nanomedicine (Lond)* **7** 855

41. Semmler-Behnke M, Kreyling WG, Lipka J, Fertsch S, Wenk A, Takenaka S, Schmid G, Brandau W 2008 *Small* **4** 2108

42. Hussain SM, Hess KL, Gearhart JM, Geiss KT, Schlager JJ 2005 *Toxicol In Vitro* **19** 975

43. Brown, DM, Johnston, H, Gubbins, E, Stone, V 2014 *Journal of Biomedical Nanotechnology* **10** 3416

44. Kermanizadeh A, Gaiser BK, Ward MB, Stone V 2013 *Nanotoxicology* **7** 1255

*45. Kermanizadeh A, Brown DM, Hutchison GR, Stone V 2013 J Nanomed Nanotechol **4** 157*

46. Jacobsen NR, Pojano G, Wallin H, Jensen KA 2010 Natl Res Centre Working Environ 6: Internal ENPRA report P1–10

47. Downes AR, Mouras R, Elfick APD 2009 *Journal of Raman Spectroscopy* **40** 757

48. Beddoes CM, Case CP, Briscoe WH 2015 *Adv Colloid Interface Sci* **218** 48

49. Chithrani DB 2010 *Mol Membr Biol* **27** 299

50. Kettler K, Veltman K, van de Meent D, van Wezel A, Hendriks AJ 2014 *Environ Toxicol Chem* **33** 481

51. Chithrani BD, Ghazani AA, Chan WC 2006 *Nano Lett* **6** 662

52. Ma N, Ma C, Li C, Wang T, Tang Y, Wang H, Moul X, Chen Z, Hel N 2013 *J Nanosci Nanotechnol* **13** 6485

53. Pezacki JP, Blake JA, Danielson DC, Kennedy DC, Lyn RK, Singaravelu R 2011*Nat Chem Biol* **7** 137

54. Mouras R, Bagnaninchi P, Downes A, Elfick A 2013 *J Raman Spec* **44** 1373

55. Mouras R, Rischitor G, Downes A, Salter D, Elfick A 2010 *J Raman Spec* **41** 848

56. Matthäus C, Chernenko T, Diem M, 2007 *Biophys J* **93** 668

57. Parekh SH, Lee YJ, Aamer KA, Cicerone MT 2010 *Biophys J* **99** 2695

58. Elsaesser A, Taylor A, de Yanés GS, McKerr G, Kim EM, O'Hare E, Howard CV 2010 *Nanomedicine (Lond)* **5** 1447

59. Ahmad Khanbeigi R., Kumar A. , Sadouki F, Lorenz C., Forbes B., Dailey LA, 2012 *J Control Release* **162** 259

60. Teeguarden JG, Hinderliter PM, Orr G, Thrall BD, Pounds JG 2007 *Toxicol Sci* **95** 300

61. Stone V, Pozzi-Mucelli S, Tran L, Aschberger K, Sabella S, Vogel U, Poland C, Balharry D, Fernandes T, Gottardo S, Hankin S, Hartl MG, Hartmann N, Hristozov D, Hund-Rinke K, Johnston H, Marcomini A, Panzer O, Roncato D, Saber AT, Wallin H, Scott-Fordsmand JJ 2014 *Part Fibre Toxicol* **13** 9

62. Hinderliter PM, Minard KR, Orr G, Chrisler WB, Thrall BD, Pounds JG, Teeguarden JG 2010 *Part Fibre Toxicol* **7** 36

63. Summers HD, Brown MR, Holton MD, Tonkin JA, Hondow N, Brown AP, Brydson R, Rees P 2013 *ACS Nano* **7** 6129

64. Vranic S, Garcia-Verdugo I, Darnis C, Sallenave JM, Boggetto N, Marano F, Boland S, Baeza-Squiban A 2013 *Environ Sci Pollut Res Int* **20** 2761

65. Ibuki Y, Toyooka T 2012 *Methods Mol Biol* **926** 157

66. Zucker RM, Massaro EJ, Sanders KM, Degn LL, Boyes WK 2010 *Cytometry A* **77** 677

67. Chen W, Liu P, Zhang A, Ren J, Xu LX 2006 *Conf Proc IEEE Eng Med Biol Soc* **1** 1478

68. Elsaesser A, Barnes CA, McKerr G, Salvati A, Lynch I, Dawson KA, Howard CV 2011 *Nanomedicine (Lond)* **6** 1189-98

69. Kreyling WG, Semmler-Behnke M, Seitz J, Scymczak W, Wenk A, Mayer P, Takenaka S, Oberdörster G 2009 *Inhal Toxicol* **21** 55

70. Singh R, Pantarotto D, Lacerda L, Pastorin G, Klumpp C, Prato M, Bianco A, Kostarelos K 2006 *Proc Natl Acad Sci U S A* **103** 3357

71. Schleh C, Semmler-Behnke M, Lipka J, Wenk A, Hirn S, Schäffler M, Schmid G, Simon U, Kreyling WG 2012 *Nanotoxicology* **6** 36